Journal of Radioanalytical and Nuclear Chemistry (2023) 332:4029–4046
https://doi.org/10.1007/s10967-023-09119-5

Different behavior of uranium(VI) on two clay minerals: montmorillonite and kaolinite

Bo Zhang[1] · Bai Gao[1,2] · Wenjie Ma[1] · Shiqi Wang[1] · Wenbin Qi[1] · Junzhe Wu[1] · Rong Wang[1] · Yujuan Zhou[1] · Yuanyuan Liu[1]

Received: 18 April 2023 / Accepted: 12 August 2023 / Published online: 14 September 2023
© Akadémiai Kiadó, Budapest, Hungary 2023

Abstract

This study investigated the feasibility of using montmorillonite and kaolinite to remediate uranium-contaminated groundwater. The results showed that the two minerals achieved U(VI) removal rates of 78.68% and 69.89%, respectively. The maximum saturation adsorption amounts were 3.78×10^{-5} mol g^{-1} and 3.85×10^{-5} mol g^{-1}, respectively. The Langmuir model and pseudo-second-order kinetics can describe the adsorption process of kaolinite on U(VI). The adsorption process of montmorillonite on U(VI) was well-fitted by Freundlich, and pseudo-second-order models. Thermodynamic parameters indicated that the two minerals' adsorption of U(VI) was a heat-absorbing reaction. The results of SEM–EDS, FT-IR revealed that the adsorption of U(VI) by the two minerals was mostly an ion-exchange reaction, and various functional groups were involved in the adsorption process. XPS results showed valence changes accompanied by kaolinite adsorption of U(VI). Montmorillonite and kaolinite have some differences in the adsorption process of U(VI).

Keywords Uranium · Montmorillonite · Kaolinite · Adsorption · Differences

Introduction

With the continuous development of human society, the demand for resources has increased. As the essential source material for nuclear industry production, the demand for uranium has been increasing, and it has been widely used in recent years [1, 2]. The enormous reserves of uranium ore in waste rocks and tailings sands release many radionuclides and other heavy metals during rainfall drenching, which harms the mine site and the surrounding soil and water environment [3]. Uranium usually exists in the environment in two states, tetravalent U(IV) and hexavalent U(VI). However, due to the high mobility of U(VI) [4] and the acid and alkaline leaching methods used to process uranium [5, 6], it is more easily released into the environment than U(IV). Due to long-term accumulation, concealment, and the lagging nature of radioactive contamination [7], methods for effectively controlling the contaminants found in the groundwater in and around uranium mines are urgently needed in the nuclear industry and environmental management fields.

^{238}U is a naturally occurring isotope of uranium [8] with a globally accepted concentration of about 0.3 μg/L [9], and the World Health Organization recommends an acceptable limit of 15 μg/L for the uranium content in drinking water [10]. In addition to the radiological hazards, uranium is also chemically toxic. The accumulation of uranium affects the environment and causes severe damage to humans, and it can be transferred to or enter the human body directly or through the food chain [11]. In recent years, various methods have been developed for removing, immobilizing, or isolating the contaminants in groundwater during remediation. The three main methods include ex-situ remediation, natural attenuation, and in-situ remediation [12]. As one of the most promising in situ remediation technologies in recent years, permeable reactive grid technology has been widely used in the remediation of contaminated groundwater [13], and the adsorbent materials most commonly used to remediate the

✉ Bai Gao
gaobai@ecit.cn

✉ Wenjie Ma
wenjiema@ecut.edu.cn

1 School of Water Resources and Environmental Engineering, East China University of Technology, Nanchang 330013, China

2 State Key Laboratory of Nuclear Resources and Environment, East China University of Technology, Nanchang 330013, China

groundwater in uranium mines include iron-based materials, cross-linked chitosan, carbonaceous materials, and agricultural wastes [14]. Most of these materials have many problems and cannot be widely used. Clay minerals are characterized by large specific surface areas, high cation exchange capacities, and low costs, and they exhibit efficient adsorption of heavy metal pollutants in addition to the variable charges present on their surfaces; this contributes to the adsorption and precipitation of radionuclide uranium ions and then controls the migration and enrichment of uranium in aqueous solutions [15, 16].

Many scholars have studied clay minerals for use with non-radioactive contaminants, complex radionuclides and heavy metal contaminants found in contaminated groundwater such as that at uranium mines. Diwan et al. [17] studied the effect of temperature on the removal of U(VI) from the aqueous phase by natural dolomite, and the results showed that natural dolomite had a significant ability to treat U(VI) contaminated water. Kornilovych et al. [18] studied the use of three clay minerals loaded with nanosized zero valent iron to adsorb U(VI) compounds in the surface and groundwater. The composite adsorbents exhibited more efficient adsorption of uranium from the surface and groundwater. Xiong et al. [19] developed a $FeSO_4$-coated magnetic biocalcium carbonate material to effectively remove uranium and europium from aqueous solutions. Shamshad et al. [20] investigated the relationship between the adsorption activity of zeolite and the chemical forms of U(VI) and Eu(III) with static experiments. Their results showed that adsorption of U(VI) and Eu(III) on the zeolite was dominated by surface complexation at pHs less than 8; the adsorption capacity of the adsorbents were 50.00 mg g^{-1} and 24.39 mg g^{-1}, respectively, indicating that zeolites are ideal materials for uranium mine remediation. Agnieszka et al. [21] studied the adsorption of U(VI) ions on seafoam and odtma-seafoam with static adsorption methods. The results showed that the modified seafoam provided more effective adsorption of U(VI), and the amount of U(VI) adsorbed by the odtma-seafoam was 285.6 mg g^{-1}. The amount of U(VI) adsorbed by the original seafoam was 142.8 mg g^{-1}.

Montmorillonite, a typical 2:1 type silicate mineral, has a tetrahedral sheet between two octahedral sheets [22]. The Mg^{2+} ions in the octahedra are replaced by Fe^{2+}, Fe^{3+}, Al^{3+}, etc.; this usually involves low-valent metal cations displacing high-valent cations, which generates a negative charge on the structural sheet layer, so the interactions of montmorillonite with the other cations in aqueous solution leads to the exchange of ions in the original layer with those in solution. In addition, chemical species can also interact reversibly with the interlayer via intermolecular hydrogen bonds, van der Waals forces, and other forces [23, 24]. Kaolinite is a typical 1:1 layered silicate mineral consisting of a layer of silica-oxygen tetrahedra and a layer of aluminum-oxygen octahedra. Its cation exchange capacity originates from dissociation of the hydroxyl groups in the crystal structure and the broken bonds at the grain edges, which are relatively low in kaolinite. The crystallinities of the grains and minerals strongly influence the cation exchange capacity of kaolinite [25].

In this paper, montmorillonite and kaolinite were selected as the research objects. The objectives of this study were (1) to investigate U(VI) adsorption by the two minerals through static experiments and to explore the differences in U(VI) adsorption by the two minerals, (2) to describe the adsorption process of U(VI) with a kinetic adsorption model and an isothermal adsorption model, and (3) to reveal the mechanism for U(VI) adsorption on the two minerals through microscopic studies of the interfacial characteristics.

Materials and methods

Materials and reagents

In this study, typical 2:1 clay minerals-montmorillonite and 1:1 clay minerals-kaolinite were selected as the subjects for the experiments, and the clay minerals used in the experiments were all extracted from the Huashuo Ore Processing Plant in Hebei Province. The physical phase compositions of montmorillonite and kaolinite were analyzed by X-ray diffraction, and the spectral peaks for montmorillonite corresponded to those in the card 00-12-0232, with 2θ of 7.43°, 19.59°, 34.33°, 54.25°, 61.365°, etc. These are the characteristic diffraction peaks of montmorillonite. The spectral peaks for kaolinite corresponded to the card 00-058-2005, and a semi-quantitative XRD analysis showed that the content of kaolinite was about 91.8 wt%.

Uranium trioxide octahydrate U_3O_8 (China National Nuclear Corporation) was used as the starting material. Sodium hydroxide (NaOH), hydrochloric acid (HCl), nitric acid (HNO_3) and sodium chloride (NaCl) were obtained from Xilong Chemical Co. All reagents were of analytical grade. At the end of the experiment, the centrifuge tube was allowed to stand for 10 min, and the supernatant was passed through a 0.25 μm aqueous filter tip, and then the U(VI) data were measured by Agilent 5100 ICP-OES. In this study, SEM–EDS analysis was performed by ZEISS Sigma 300 from Germany, FT-IR was performed by Thermo Scientific Nicolet iS20 from the United States, XPS was performed by Thermo Scientific K-Alpha from the United States, and XRD was performed by Rigaku Smart Smart K-Alpha from Japan.

Batch adsorption experiments

Experiments designed to determine the effect of solution pH on the adsorption of U(VI) by minerals: U(VI) solutions

with concentrations of 4.2×10^{-5} mol L^{-1} and pH values of 2.0 ± 0.1, 3.0 ± 0.1, 4.0 ± 0.1, 5.0 ± 0.1, 6.0 ± 0.1, 7.0 ± 0.1, 8.0 ± 0.1, 9.0 ± 0.1, 10.0 ± 0.1 were prepared; adsorbent was weighed and added into a plastic tube containing 50 mL of a U(VI) solution with one of the above pH values. The sample was shaken (220 r min^{-1}) for 24 h and then analyzed. The pH of the solution was adjusted by slowly adding a HNO_3 standard solution with a concentration of 0.1 mol L^{-1} or a NaOH standard solution with a concentration of 0.1 mol/L. The temperature of the system was maintained at 25 °C ± 0.5 °C.

Experiment on the effect of reaction time on adsorption of U(VI) by the minerals. These experiments investigated the effect of reaction time on adsorption with four solid concentrations: the solution pH was 6.0 ± 0.1, the concentration of the U(VI) solution was 4.4×10^{-5} mol L^{-1}, the solid concentrations were 0.5 g L^{-1}, 1.0 g L^{-1}, 2.0 g L^{-1}, 3.0 g L^{-1}, and the reaction times were 0.17 h, 0.5 h, 1 h, 2 h, 6 h, 12 h, 15 h, 24 h, 36 h, and 48 h. The pH and system temperature were adjusted as above.

Effect of the initial concentration on U(VI) adsorption by minerals. These experiments investigated the effect of initial concentration on adsorption at three system temperatures. The pH of the configured solution was 6.0 ± 0.1, the initial concentrations of the U(VI) solutions were 1.3×10^{-5} mol L^{-1}, 2.1×10^{-5} mol L^{-1}, 3.0×10^{-5} mol L^{-1}, 4.2×10^{-5} mol L^{-1}, 6.3×10^{-5} mol L^{-1}, 8.2×10^{-5} mol L^{-1}, and 1.3×10^{-4} mol L^{-1}, the reaction temperatures were 298.15 K, 308.15 K, and 318.15 K, and the reaction times were 24 h. The pH and system temperature were adjusted as above. Three parallel samples and one blank sample without minerals were set up for each group of experiments.

The adsorption capacities and U(VI) removal rates of the minerals are important parameters used in studying the adsorption of U(VI) by the minerals, and the calculations were performed as shown below:

$$Q = \frac{(C_0 - C_t)\times V}{m} \tag{1}$$

$$S = \frac{(C0 - Ct)}{C0}\times 100\% \tag{2}$$

where Q is the adsorption volume, mol g^{-1}; m is the dosage, g; V is the solution volume, L; S is the removal rate, %; C_0 is the initial concentration of pollutant, mol L^{-1}; and C_t is the concentration of the pollutant at time t, mol L^{-1}.

Results and discussion

Effect of pH

The active sites on the surfaces of clay minerals are the primary sites for adsorption of contaminants by minerals. Their protonation-deprotonation reactions, as well as the lamellar charges, are affected by the pH of the solution. At the same time, the pH also determines the forms of uranium present in the aqueous solutions, so the pH is the main factor affecting the adsorption of uranium on the clay minerals. The forms of U(VI) present in aqueous solutions with the different pH values used in the experiments were simulated with Visual Minteq 3.1, and the results are shown in Fig. 1. Under these experimental conditions, the uranium in solution was mainly U(VI). When the solution pH was 2.0–3.0, the U(VI) was mainly of the form UO_2^{2+} with a content of more than 99%, and when the pH of the solution was greater than 3, U(VI) predominated. The U(VI)

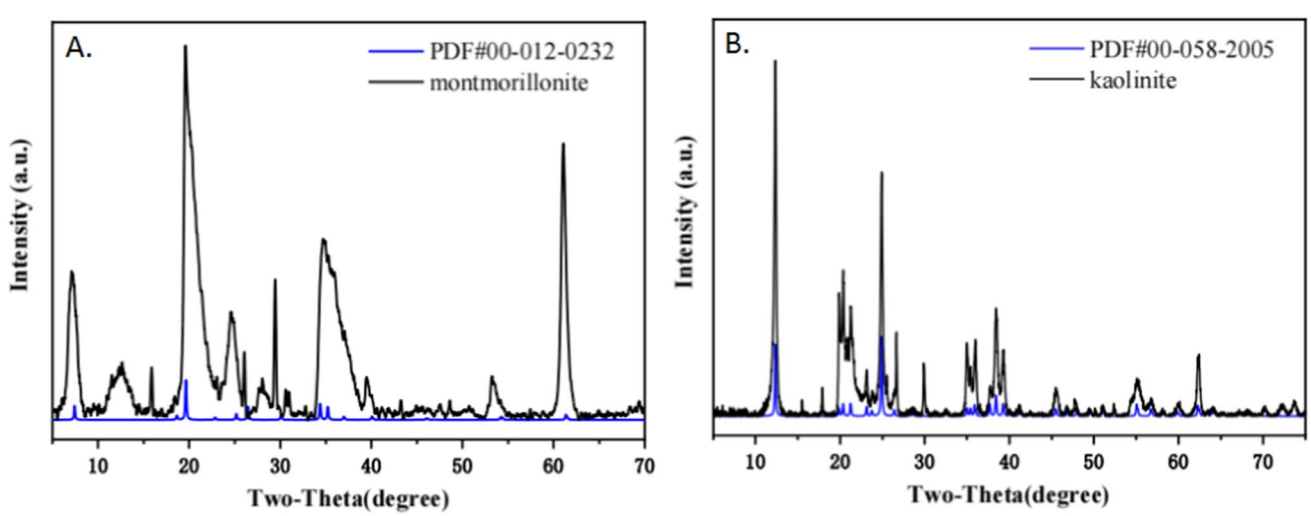

Fig. 1 XRD patterns for vermiculite, montmorillonite and kaolinite

species were $(UO_2)_3(OH)_5^+$ and $(UO_2)_4(OH)_7^+$ and other uranyl groups with OH^- ligands. When the solution pH was approximately 6.5, the U(VI) in solution was mainly present as cationic uranyl ions. The largest proportion was that of $(UO_2)_3(OH)_5^+$ at about 76.8%. When the pH of the solution was greater than 7, U(VI) started to form uranyl anions such as $(UO_2)_3(OH)_7^-$ and $UO_2(OH)_3^-$. The largest percentage of uranyl anions, about 92.2%, was observed when the pH was increased to 9 (Fig. 2).

The amount of U(VI) adsorbed by kaolinite reached its best at pH 7, with an adsorption amount of 6.02×10^{-5} mol g^{-1} and a removal rate of 69.89%, as seen in Fig. 3A. When the pH was less than 7, the amount adsorbed increased gradually with increasing pH. As the pH increased, the Zeta potential of the adsorbent surface gradually increased and negative charges accumulate on the adsorbent surface (Fig. 4). At this time, the uranium species in solution were mainly $(UO_2)_3(OH)_5^+$, $(UO_2)_4(OH)_7^+$, $(UO_2)_3(OH)_7^-$, and $UO_2(OH)_3^-$ [26], and the adsorption of U(VI) by kaolinite may have involved internal coordination or surface precipitation. When the pH continued to increase and became alkaline, U(VI) was precipitated as the insoluble heavy uranate salt ($Na_2U_2O_7$) (Fig. 5). The surface precipitation maintained the percent of U(VI) adsorbed on kaolinite at a high level [27].

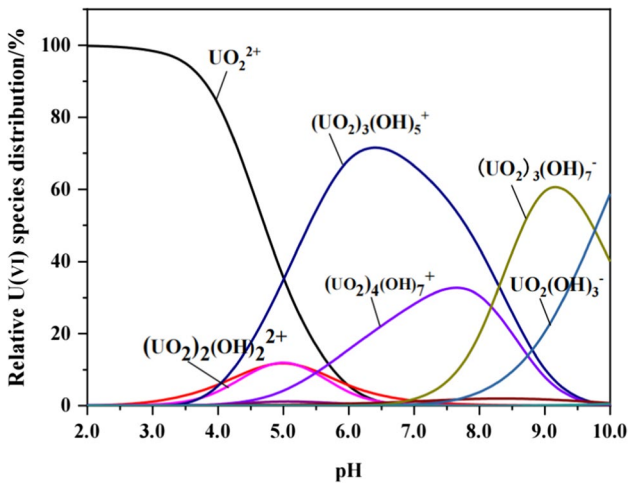

Fig. 2 The forms of U(VI) present in aqueous solutions with different pH values

Figure 3B shows that the amount of U(VI) adsorbed on montmorillonite reached its best when the pH was 5. The adsorption amount was 6.78×10^{-5} mol g^{-1}, the removal rate was 78.68%, and the adsorption efficiency increased rapidly when the pH was higher than 3 and decreased sharply when the pH value was greater than 7, so the best pH range for U(VI) adsorption on montmorillonite was 4–7. When the pH was less than 4, the degree of montmorillonite surface deprotonation was not high, and deprotonation ($-H^+$) was difficult, which made the negative charge on the surface low. Since the uranyl species in the solution were mainly cationic, adsorption of the U(VI) acyl ions by the negative adsorption sites on the surface of montmorillonite was ineffective, and the H^+ in the solution exhibited competitive adsorption with the uranyl cations, so the adsorption percentages at this stage were small; when the pH was increased to 4–7, the amount of U(VI) adsorbed on the montmorillonite increased, and the uranyl ions in the solution at this time were mainly $(UO_2)_3(OH)_5^+$ and $(UO_2)_4(OH)_7^+$. This indicated that uranium was mainly adsorbed as $(UO_2)_3(OH)_5^+$ and $(UO_2)_4(OH)_7^+$ when the pH was 4–7; when the pH was greater than 7, the Zeta potential on the surface of the adsorbent was elevated due to deprotonation of the oxygen-containing functional groups on the surface, and OH^- increases the concentration of negative charges on the surface of the adsorbent. At this time more montmorillonite sites were deprotonated, and uranyl anions were formed in the solution. The amount of U(VI) adsorbed by montmorillonite began

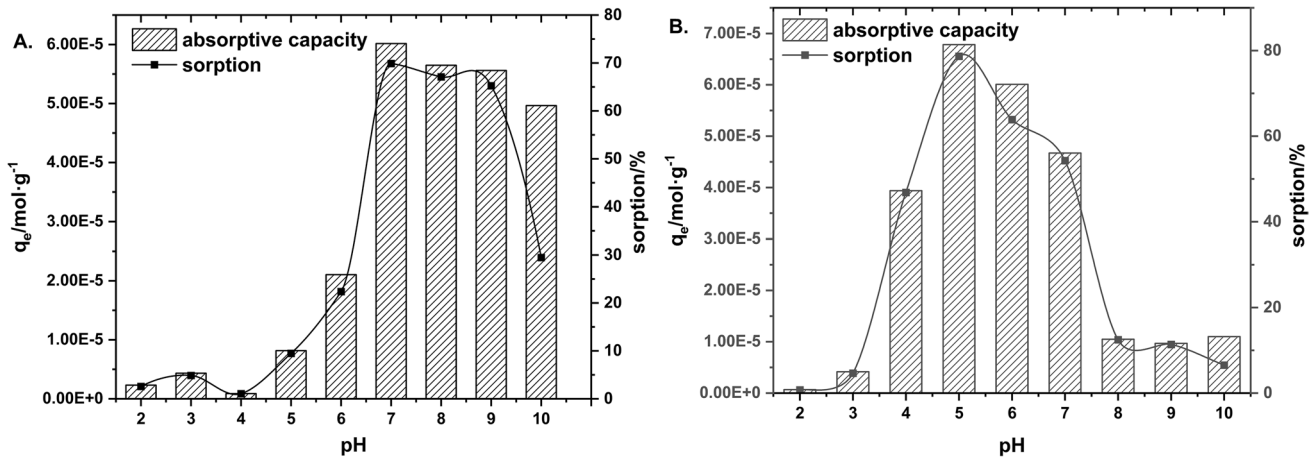

Fig. 3 Relationship between the adsorption capacity of U(VI) and the pH. *Note* **A** kaolinite **B** montmorillonite

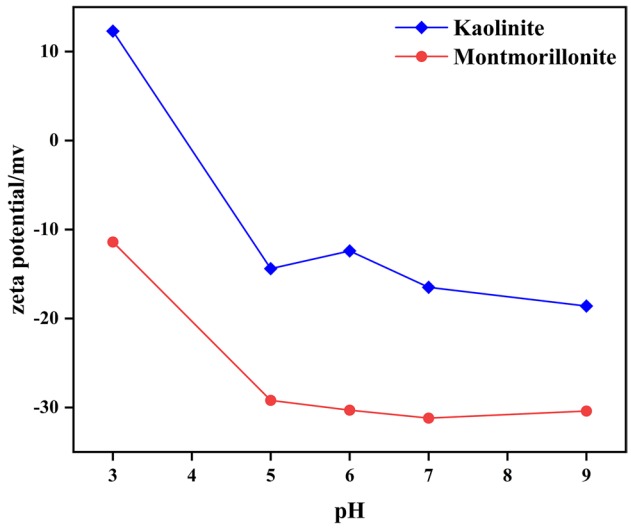

Fig. 4 Zeta potential of adsorbents at different pH values

to decline, and many negative charges accumulated on the surface (Fig. 5); these repelled the uranyl anions in solution leading to a decrease in adsorption [28].

Effect of reaction time

When the solid concentration was the same, the amounts of U(VI) adsorbed by the montmorillonite and kaolinite gradually increased with increasing reaction time and finally reached equilibrium. The amount of U(VI) adsorbed on both minerals on gradually decreased with increased solid concentrations. This occurred because during the reaction, the concentration of solid increased after reaching adsorption saturation, the amount adsorbed was relatively lower, and the sample particles used in this study were less than 100 mesh or 200. Some of the solid particles with small particle sizes diffused into the liquid phase to produce colloids, complexes, and fine particles, which formed complexes or bonds with U(VI); the bonds with the small particles were difficult to separate from the liquid phase when the solid–liquid separation was carried out, so they remained in the liquid phase and exhibited competitive adsorption with U(VI) on the solid surface, which decreased the amount adsorbed on the solid. When the solid concentration was 0.5 g L^{-1}, the adsorption of kaolinite on U(VI) reached equilibrium after about 6 h. At this time, the maximum adsorption amount was 2.78×10^{-5} mol g^{-1}. The amount of U(VI) adsorbed on montmorillonite reached equilibrium at 5.63×10^{-5} mol g^{-1} after about 12 h of reaction time. The equilibrium times for adsorption of U(VI) on montmorillonite and kaolinite were increased when the solid concentration increased, which is because the spaces between the solid particles decreased after the solid concentration in the system increased, which intensified the collisional friction between the particles and accelerated the rates of the solid particle reactions with uranium (Figs. 6 and 7).

Effect of initial concentration

As shown in Fig. 8, the amount of U(VI) adsorbed on both montmorillonite and kaolinite increased with increases in the initial concentration of U(VI) in the solution, and the removal rate of U(VI) was reversed. When there were enough adsorption sites on the solid surfaces in the system, the increased concentration of U(VI) ions in the system filled each adsorption site, so when the initial concentration increased, the amount adsorbed also gradually increased, but the number of adsorption sites on the solid surface were limited. After the adsorption concentration reached a certain level, the adsorption sites were saturated. Therefore, the removal rate gradually decreased with increases in the initial concentration. In addition, at higher temperatures, the amount U(VI) adsorbed by both minerals at different initial concentrations increased, and the adsorption rates increased, indicating that the increased temperature promoted adsorption of the U(VI) on both minerals; the adsorption may be a heat-absorbing reaction, or the higher temperature accelerated the diffusion of U(VI) ions outside the solid boundary layer as well as in the pores inside the particles, thus contributing to the increased adsorption capacity (Figs. 9, 10, and 11).

Adsorption isotherms

Isothermal adsorption models are commonly used to describe the adsorption process and evaluate the adsorption capacity. The commonly used isothermal adsorption models are the Langmuir, Freundlich, Temkin, and D-R models [29].

The Langmuir model assumes that the adsorbent surface is homogeneous, the activation energy of each molecule on the adsorbent surface is equal, and the adsorption process is homogeneous monolayer adsorption. The expressions are as follows:

$$\frac{Ce}{qe} = \frac{1}{KL + q\max} + \frac{Ce}{q\max} \tag{3}$$

$$RL = \frac{1}{1 + KL \times C0} \tag{4}$$

where C_e is the equilibrium concentration of the pollutant, mol L^{-1}; C_0 is the initial concentration of the pollutant, mol L^{-1}; q_e is equilibrium adsorption, mol g^{-1}; q_{max} is maximum monolayer coverage, mol g^{-1}; K_L is a model constant, L mol^{-1}; and R_L is an equilibrium parameter. $R_L = 0$ means

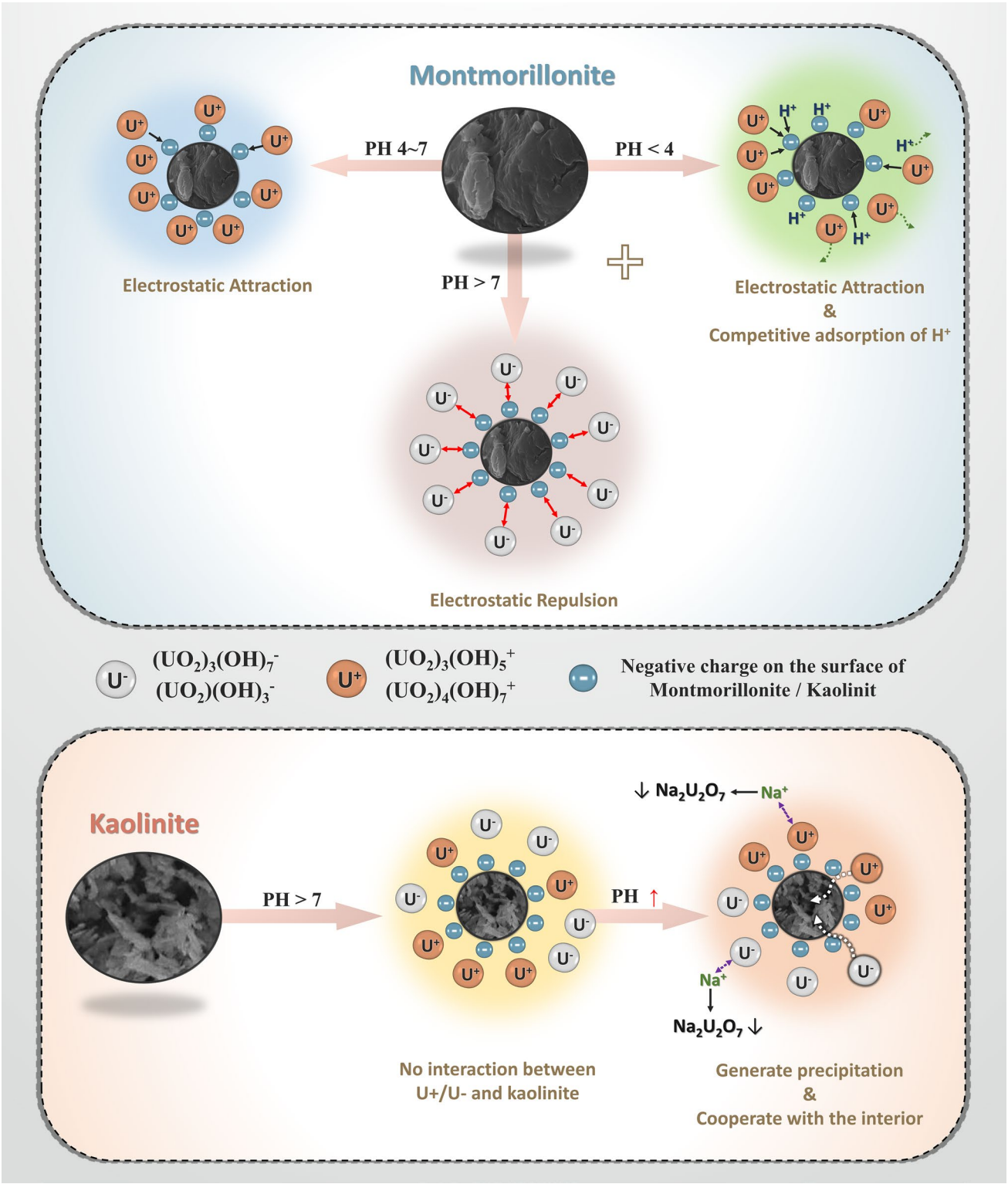

Fig. 5 Interaction of uranium ore with adsorbent

the adsorption process is irreversible, $0 < R_L < 1$ means monolayer adsorption dominated, and $R_L > 1$ indicates monolayer adsorption was poor (Figs. 12, 13, and 14).

The Freundlich model assumes complex interrelationships among the molecules on the adsorbent surface and that the adsorption process is non-homogeneous multilayer adsorption [30]. The expression is as follows:

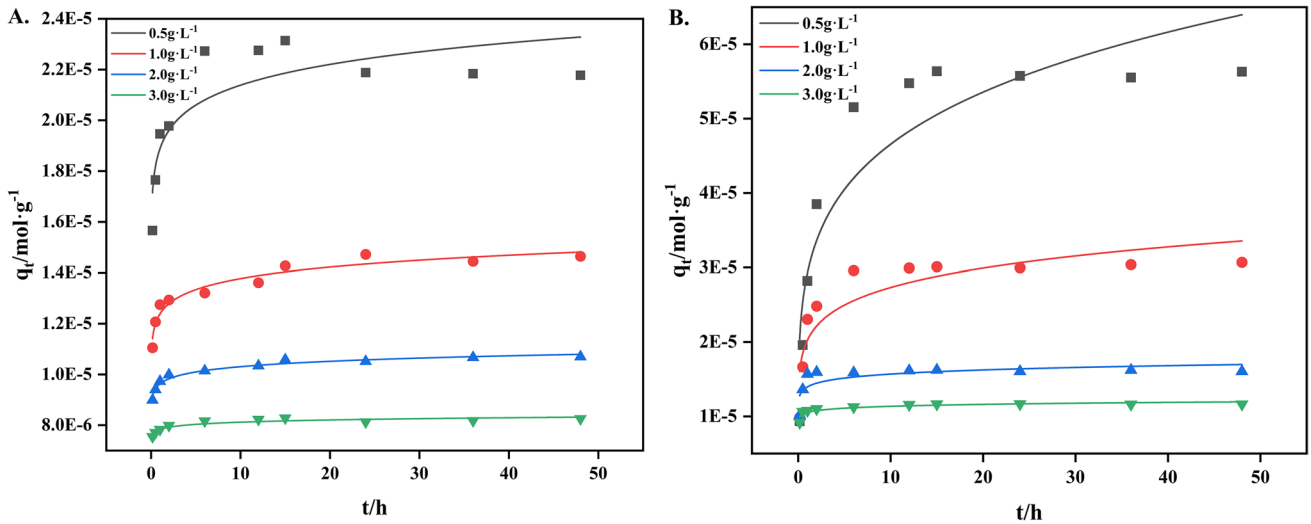

Fig. 6 Relationship between the U(VI) adsorption capacity and the adsorbent concentration. *Note* **A** kaolinite **B** montmorillonite

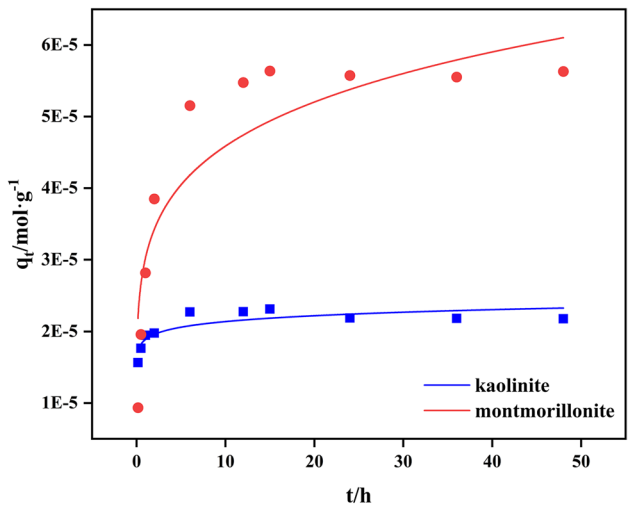

Fig. 7 Relationship between the U(VI) adsorption capacity and the reaction time. *Note* **A** Background solution; pH = 6.0 ± 0.1; adsorbent concentration = 0.5 g L^{-1}

$$\ln qe = \frac{1}{n_F} \times \ln Ce + \ln KF \tag{5}$$

where q_e indicates equilibrium adsorption, mol g^{-1}; K_F is a model constant; and n_F is an empirical parameter. n_F values between 1 and 10 indicate dominant adsorption.

The Temkin model is similar to the Freundlich isothermal adsorption model and assumes that the energy consumed by adsorption decreases linearly with adsorption and that the heat of adsorption decreases with increasing coverage and applies to systems with inhomogeneous adsorbent surfaces [31]. The expression is as follows:

$$qc = B \ln KT + B \ln Ce \tag{6}$$

where q_c is the adsorption amount, mol g^{-1}; B is a constant associated with the heat of adsorption, J mol^{-1}; and K_T is the equilibrium binding constant, L g^{-1}.

The D-R model is based on microporous filling theory with the following expressions:

$$ln\, q_c = ln\, q_m - \beta\varepsilon^2 \tag{7}$$

$$\varepsilon = RTln\left(1 + \frac{1}{c_e}\right) \tag{8}$$

$$E = \frac{1}{\sqrt{2\beta}} \tag{9}$$

where β is the activity coefficient, $mol^2\ kJ^{-2}$; R is the ideal gas constant, J (mol K)$^{-1}$; T is the absolute temperature, K; ε is the Polanyi potential; E is the average free energy, kJ mol^{-1}. E < 8 kJ mol^{-1} indicates that physical adsorption is the main mechanism of action; 8 kJ mol^{-1} < E < 16 kJ mol^{-1} indicates that ion-exchange chemisorption is the main mechanism of action; E > 16 kJ mol^{-1} indicates that chemical adsorption is the main mechanism of action (Figs. 15, 16 and 17).

The R^2 value for kaolinite with the Langmuir prediction model was high, and the maximum amount of U(VI) adsorbed was 3.58×10^{-5} mol g^{-1}. Compared with the maximum adsorption amount predicted by D-R model, the prediction of the Langmuir model was closer to the actual experimental data, which indicated that adsorption of the U(VI) on kaolinite was more consistent with the Langmuir

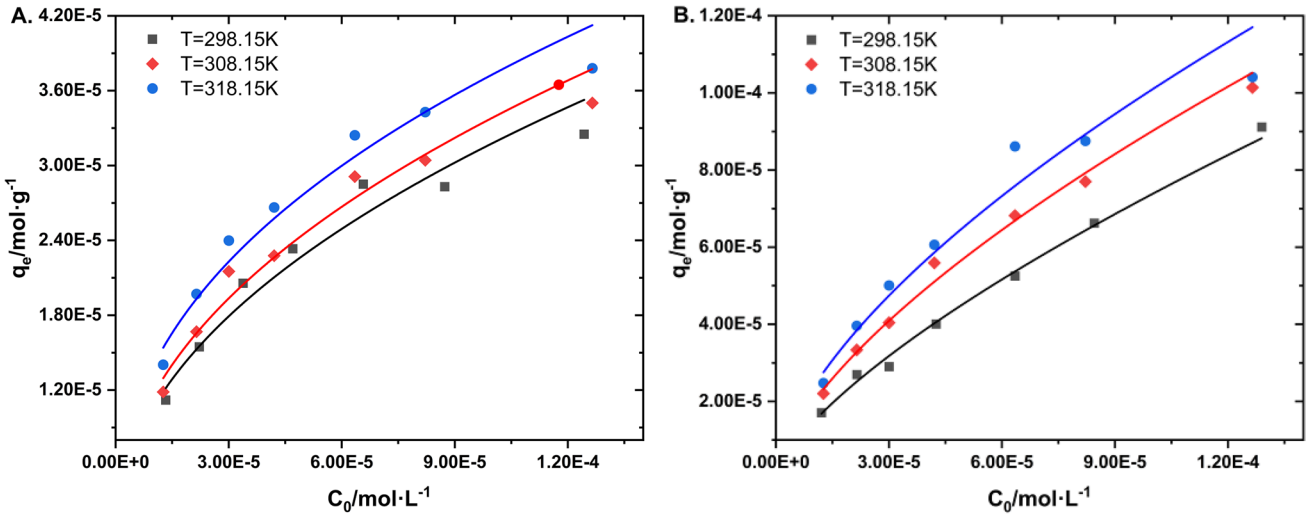

Fig. 8 Relationship between the U(VI) adsorption capacity and initial concentration. *Note* **A** kaolinite **B** montmorillonite

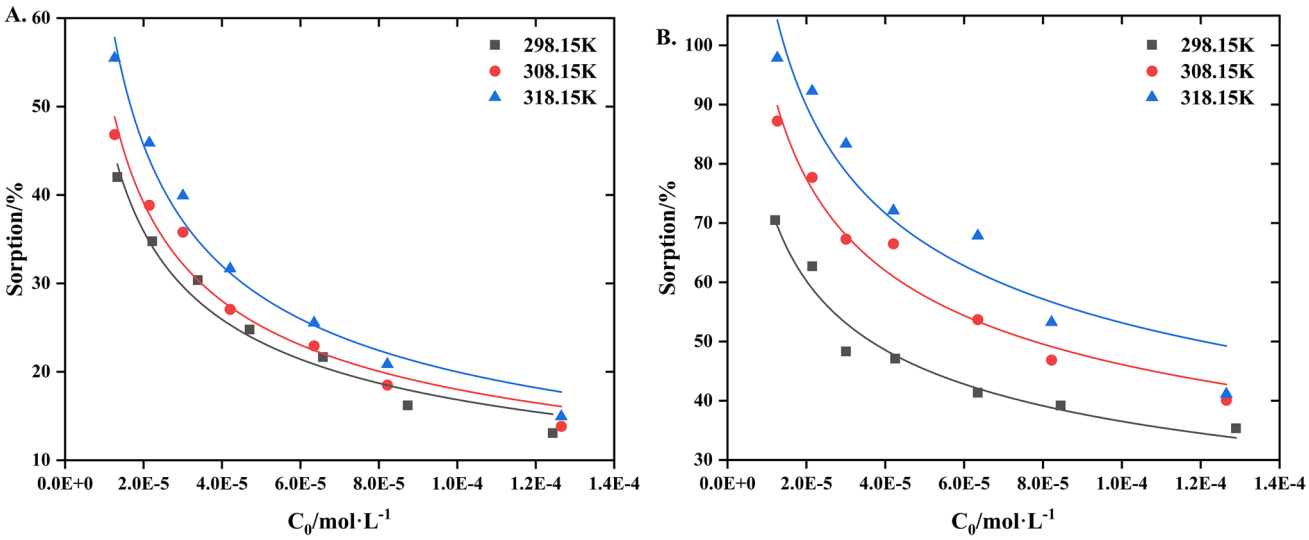

Fig. 9 Relationship between the U(VI) adsorption rate and initial concentration. *Note* **A** kaolinite **B** montmorillonite

model. The reaction mainly involved homogeneous monolayer adsorption. The amount adsorbed was related to the number of active sites on the surface of the kaolinite. The fitted E values for the kaolinite D-R model ranged from 8.0 to 16.0 kJ mol^{-1}, indicating that adsorption of the U(VI) on kaolinite was mainly an ion-exchange reaction occurring at the kaolinite edge surface sites (Tables 1, 2, and 3).

The R^2 values for montmorillonite with the Freundlich and D-R prediction models were 0.97184 and 0.96001, respectively, which were better than that of the Langmuir prediction model, proving that adsorption of the U(VI) on montmorillonite mainly occurred via multilayer inhomogeneous adsorption or pore diffusion adsorption. The separation coefficients R_L calculated with Langmuir model for the adsorption of U(VI) on montmorillonite were greater than 0. According to the Langmuir model equation, when $0 < R_L < 1$, adsorption is favorable, and the adsorption process is irreversible when $R_L = 0$. Therefore, the adsorption of U(VI) on montmorillonite was favorable and montmorillonite can be used as an adsorbent of U(VI). n is the fitting parameter used in the Freundlich model to characterize the equivalent adsorption strength, and when n is between 1 and 10, adsorption is favorable. The n value for montmorillonite was between 1 and 10, which indicated that adsorption of U(VI) on montmorillonite was favorable. The E values for U(VI) adsorption on montmorillonite ranged from 8.0 to 16.0 kJ mol^{-1}, and the adsorption mode was mainly ion exchange.

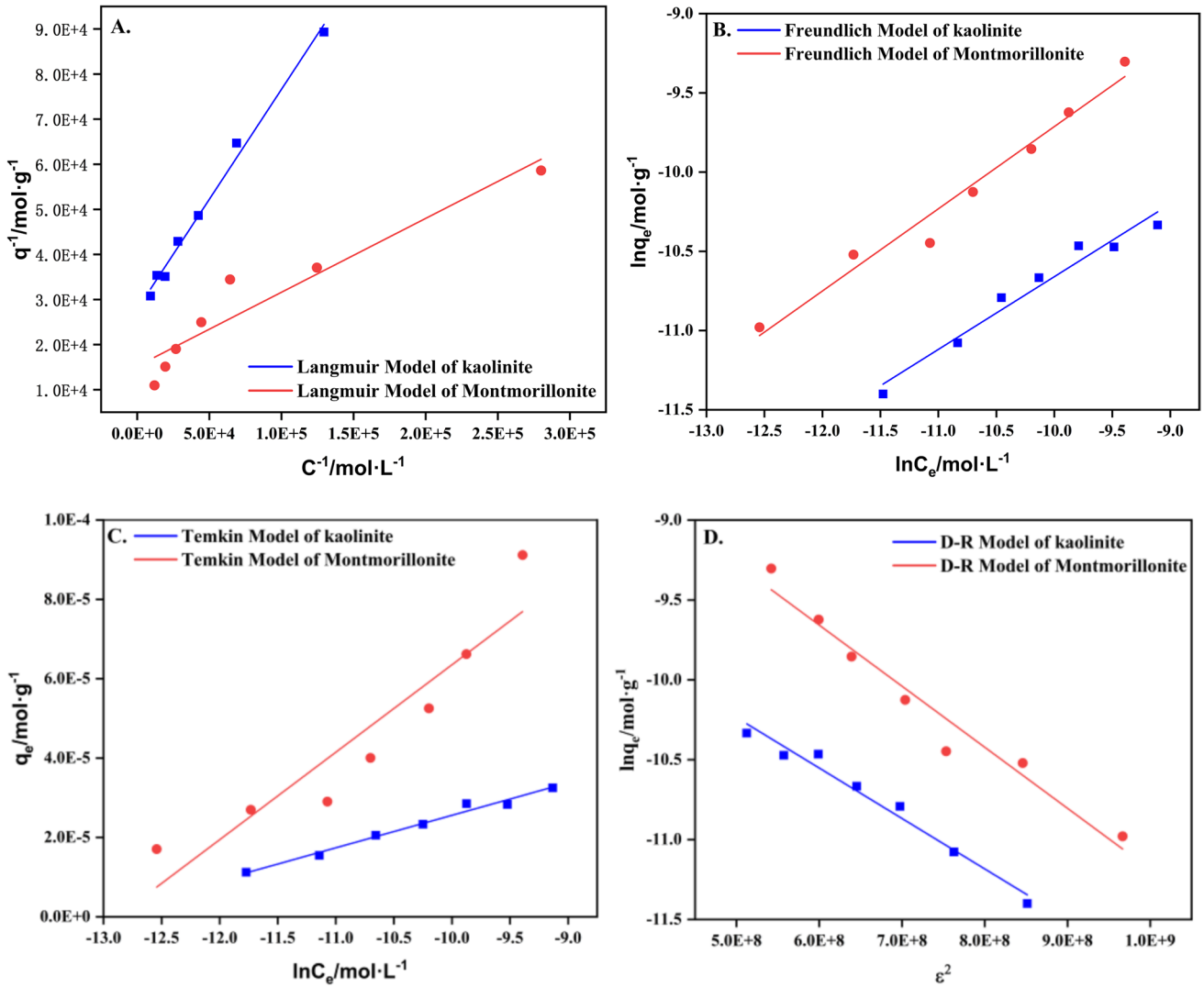

Fig. 10 Isothermal adsorption curves for U(VI) adsorption by the clay minerals. *Note* **A** Langmuir model; **B** Freundlich model; **C** Temkin model; **D** D-R model

Adsorption kinetics

Adsorption kinetic models can describe the rates for adsorption of radionuclides and heavy metals on mineral surfaces and describe the migration rates and mechanisms for the radionuclides and heavy metals [32].

The pseudo-first-order kinetic model assumes that adsorption is controlled by diffusion and is commonly used to estimate the mass transfer coefficient. The expression is as follows:

$$log\,(qe - qt) = log\,qe - \left(\frac{k1}{2.303}\right)t \tag{10}$$

where q_e is the amount adsorbed at equilibrium, mol g^{-1}; q_t is the amount adsorbed at time t, mol g^{-1}; and k_1 is the adsorption rate constant, h^{-1}.

The pseudo-second-order kinetic model assumes that the adsorption rate is proportional to the number of surface active sites. The expression is as follows:

$$\frac{t}{qt} = \frac{1}{k_2 \times qe} + \frac{t}{qe} \tag{11}$$

where k_2 is the adsorption rate constant, g (mol h)$^{-1}$.

The two-constant kinetic model, also known as Freundlich's revised formal model, considers electrostatic gravity as the main reason for rapid diffusion of the adsorbed mass, and the adsorption process is influenced by the

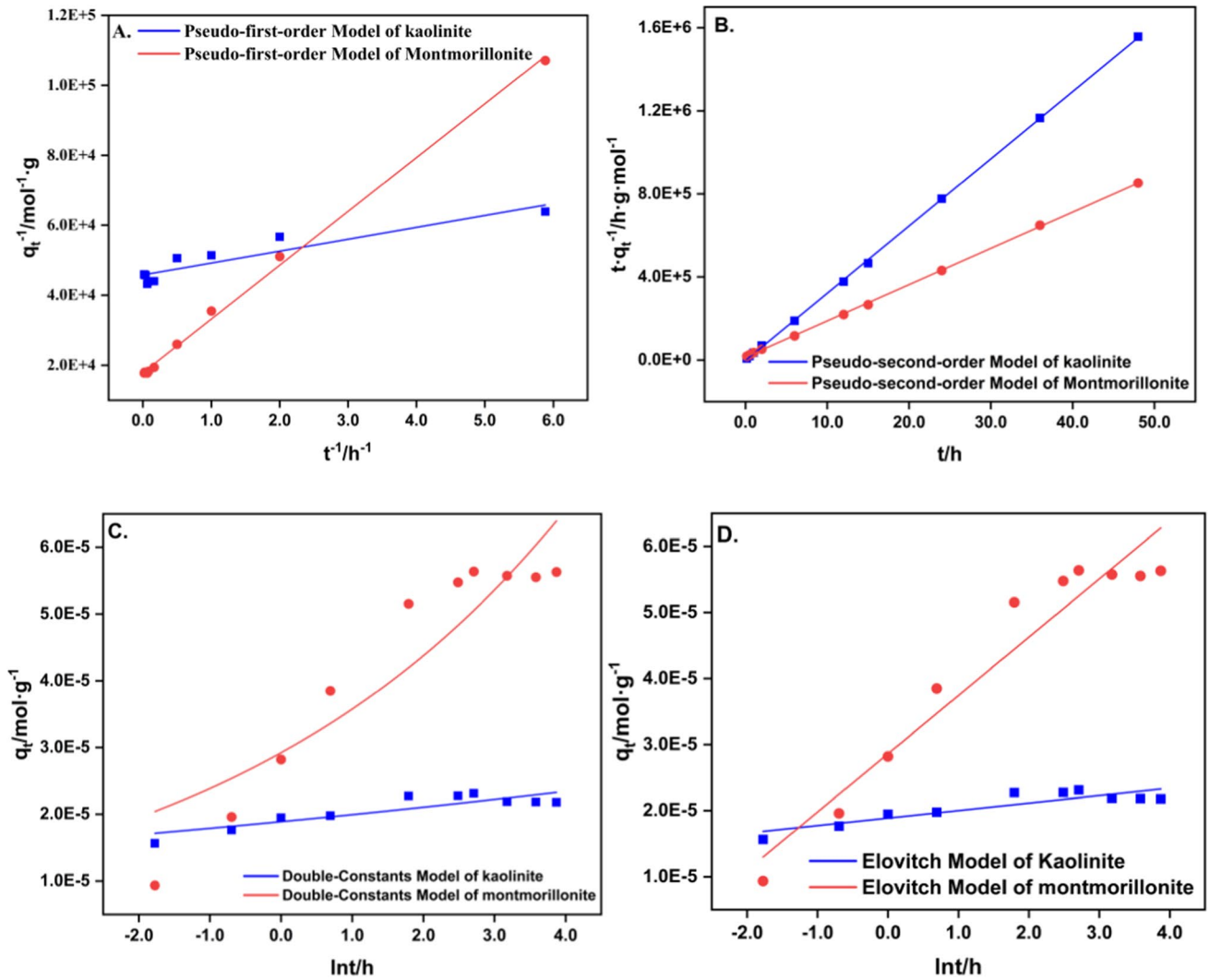

Fig. 11 Kinetic model curves for U(VI) adsorption by the clay minerals. *Note* **A** pseudo-first-order kinetic model; **B** pseudo-second-order kinetic model; **C** two-constant kinetic model; **D** Elovitch model

decrease in free energy and the increase in entropy [33]. The model can be expressed as follows:

$$q_t = e^{\alpha + k \ln t} \tag{12}$$

where a is the reaction constant, mol g^{-1}, and k is the adsorption constant, mol g^{-1}.

The Elovich kinetic model is applicable to chemically-dominated non-homogeneous diffusive adsorption processes, in which adsorption is influenced by diffusion within the liquid and on the surface, and adsorption can be accomplished by surface activation, de-activation and adsorption at the active site [34]. The expression for the model is as follows:

$$q_t = \frac{1}{\beta} ln(\alpha\beta) + \frac{1}{\beta} lnt \tag{13}$$

where α is the initial adsorption rate, mol min^{-1} g^{-1}, and β is the resolution constant, g mol^{-1}.

The adsorption of U(VI) on kaolinite was more consistent with the pseudo-second-order kinetic model. The correlation coefficient R^2 was above 0.999, indicating that chemisorption mainly controlled the rate of U(VI) adsorption on kaolinite. The correlation coefficient R^2 for U(VI) and kaolinite in the fit to the pseudo-first-order kinetic model was 0.86585, indicating that the rate of U(VI) adsorption on kaolinite was influenced by diffusion. The correlation between the adsorption of U(VI) on kaolinite via the double constant model and Elovitch model was not obvious. This indicated that, in the process of U(VI) adsorption on kaolinite, chemical effects had more influence on the adsorption process than diffusion [35].

The correlation coefficients for fits of the data to the kinetic models for the adsorption of U(VI) on

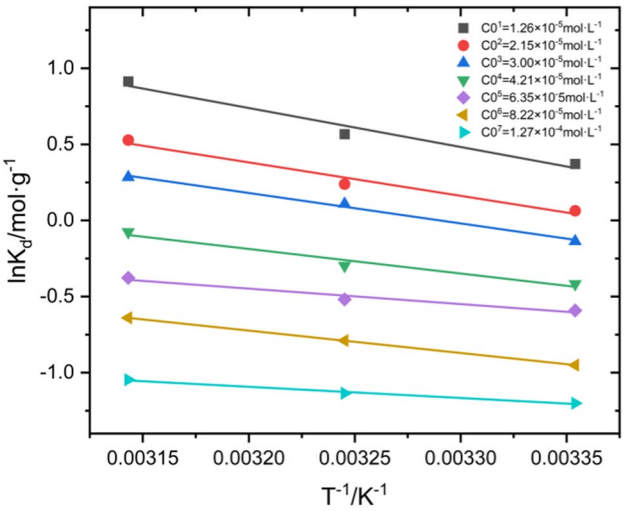

Fig. 12 Thermodynamic model fits for U(VI) adsorption by kaolinite

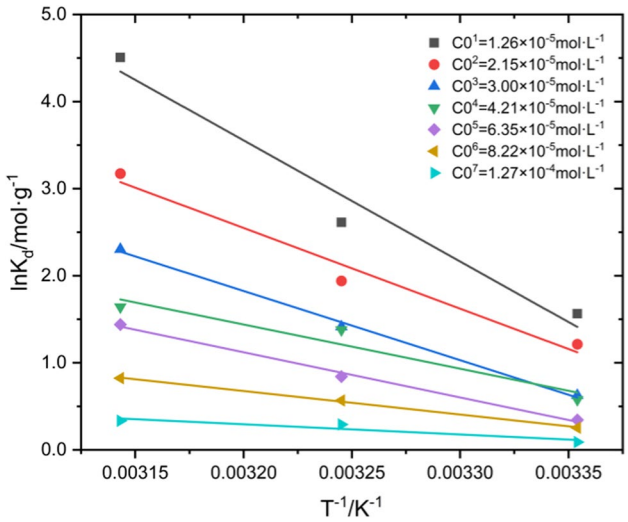

Fig. 13 Thermodynamic model curves for U(VI) adsorption on montmorillonite

montmorillonite were 0.99774 for the pseudo-first-order model, 0.99974 for the pseudo-second-order model, 0.8469 for the two-constant kinetic model, and 0.93436 for the Elovitch model. The correlation coefficients for the fits of the pseudo-first-order kinetic model and the pseudo-second-order kinetic model were both greater than 0.99, indicating that the adsorption of U(VI) on montmorillonite involved both chemisorption and physical adsorption. However, the comparison showed that the correlation coefficient R^2 for the fit to the pseudo-second-order model was more significant than those of the other three models, and the theoretical value of the equilibrium adsorption capacity (5.73×10^{-5} mol g^{-1}) is closer to the practical (5.63×10^{-5} mol g^{-1}), indicating that adsorption of U(VI) on montmorillonite mainly occurred via multilayer chemisorption. The free energy for adsorption was independent of surface coverage, and the adsorption process was also affected by diffusion.

Thermodynamic adsorption

The thermodynamic model of adsorption is mainly used to describe the thermodynamic properties of the adsorption process and provide insight into the mechanism of temperature effects on the water–rock. The mechanism for the temperature effects on adsorption reactions occurring at the water–rock interface can be understood, and the ease of adsorption can be determined from changes in the entropy and enthalpy during the reaction at a specific temperature [36]. The Van't Hoff equation is commonly used to solve for the thermodynamic parameters in the following expressions:

$$\Delta G^0 = -RT \ln Kd \tag{14}$$

$$\Delta G^0 = \Delta H^0 - T\Delta S^0 \tag{15}$$

$$\ln K_d = \frac{\Delta S^0}{R} - \frac{\Delta H^0}{RT} \tag{16}$$

where ΔG^0 (J mol^{-1}) is the Gibbs free energy, ΔH^0 (J mol^{-1}) is the enthalpy change for the reaction in the standard state, ΔS^0 (J mol^{-1} K^{-1}) is the entropy change of the reaction in the standard state, R is the thermodynamic constant $R = 8.314$ J mol^{-1} K^{-1}, and K_d is the equilibrium constant.

The thermodynamic fitting results show that the enthalpies for adsorption of U(VI) on the kaolinite surface were all positive, indicating that the adsorptions of U(VI) on kaolinite were all heat-absorbing processes; in addition, for adsorption of U(VI) on kaolinite, ΔH decreased with increases in the initial concentration of U(VI), indicating that the adsorption of U(VI) on kaolinite was dependent on temperature. During the adsorption processes, ΔS was always greater than 0. For reaction systems involving solid–liquid exchange, U(VI) loses some of its degrees of freedom when it is exchanged from the liquid phase, which has a high degree of freedom, to the solid–liquid system, and is then confined by the mineral surface, thus limiting the active space of U(VI) and leading to a change in ΔS. When the initial concentration of U(VI) was low, ΔG was negative, and the value was more negative at higher temperatures. When the adsorption of U(VI) on kaolinite was a spontaneous reaction, the energy of this spontaneous reaction was positively correlated with temperature; as the initial concentration of U(VI) was increased, ΔG became positive,

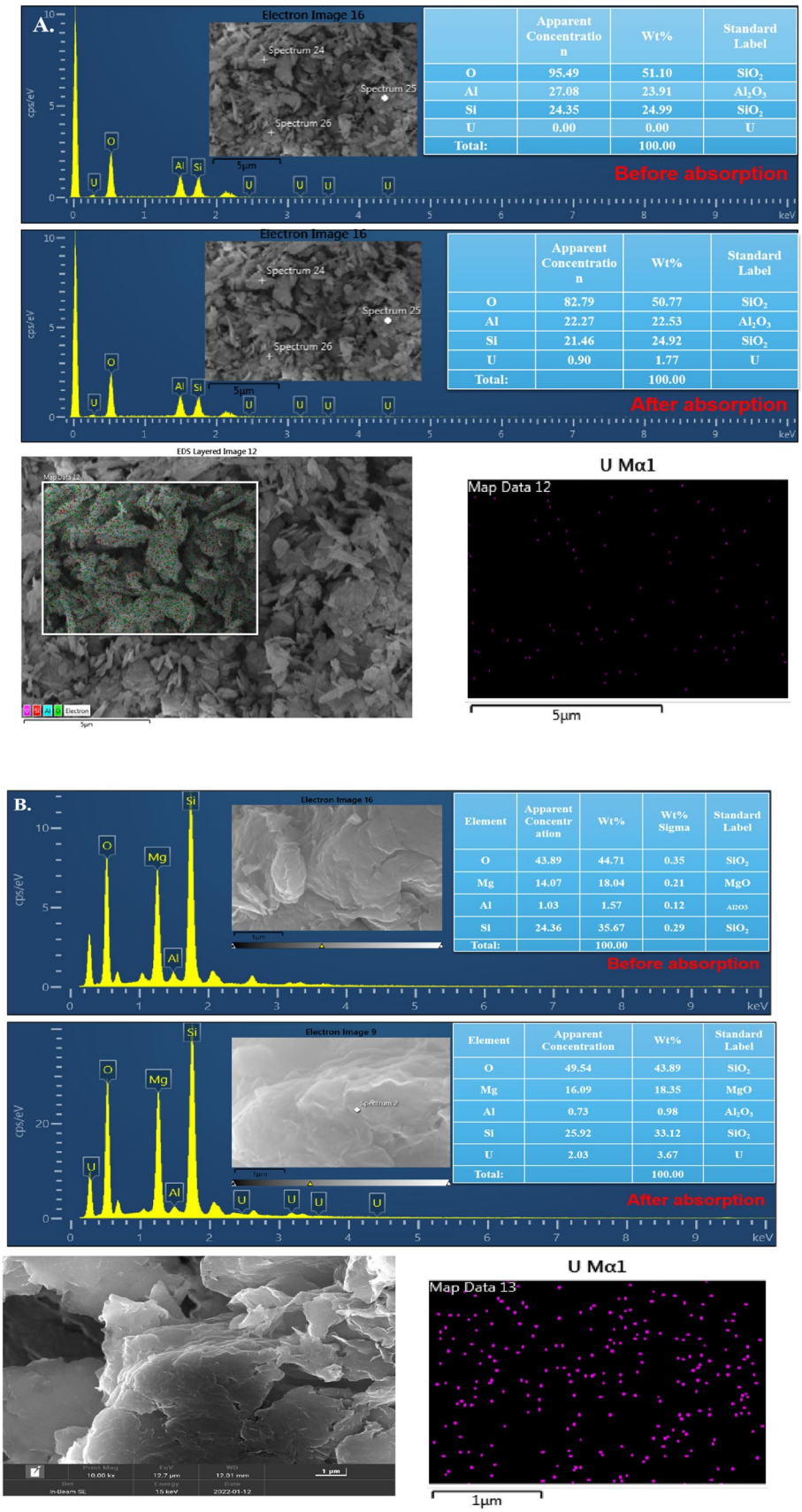

	Apparent Concentration	Wt%	Standard Label
O	95.49	51.10	SiO_2
Al	27.08	23.91	Al_2O_3
Si	24.35	24.99	SiO_2
U	0.00	0.00	U
Total:		100.00	

	Apparent Concentration	Wt%	Standard Label
O	82.79	50.77	SiO_2
Al	22.27	22.53	Al_2O_3
Si	21.46	24.92	SiO_2
U	0.90	1.77	U
Total:		100.00	

Element	Apparent Concentration	Wt%	Wt% Sigma	Standard Label
O	43.89	44.71	0.35	SiO_2
Mg	14.07	18.04	0.21	MgO
Al	1.03	1.57	0.12	Al2O3
Si	24.36	35.67	0.29	SiO_2
Total:		100.00		

Element	Apparent Concentration	Wt%	Standard Label
O	49.54	43.89	SiO_2
Mg	16.09	18.35	MgO
Al	0.73	0.98	Al_2O_3
Si	25.92	33.12	SiO_2
U	2.03	3.67	U
Total:		100.00	

Fig. 14 SEM–EDS diagram for U(VI) adsorption on the clay minerals. *Note* **A** kaolinite **B** montmorillonite (Background solution pH: 6.0 ± 0.1)

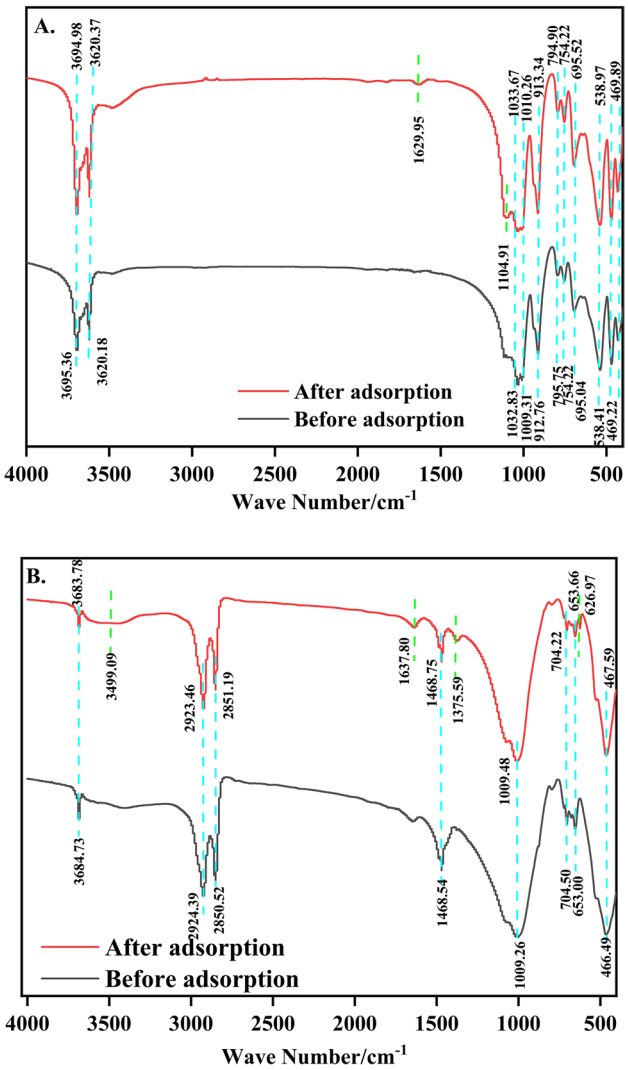

Fig. 15 FT-IR spectra for U(VI) adsorbed on the clay minerals. *Note* **A** kaolinite **B** montmorillonite (Background solution pH: 6.0 ± 0.1)

and the positive values were less with higher temperatures, indicating that when the initial concentration was increased, the adsorption of kaolinite on U(VI) required heating and was not a spontaneous reaction [37].

As shown in Table 4, ΔH was positive for the adsorption of U(VI) on montmorillonite, indicating that the adsorption of U(VI) on montmorillonite was a heat-absorbing reaction, and the increased temperature enhanced adsorption. The ΔS was positive during the adsorption of U(VI) on montmorillonite, indicating that the surface structure of the montmorillonite changed during the adsorption process, and adsorption might be controlled by the inner ligand reaction [38]. The Gibbs free energy ΔG was less than 0 for the adsorption of U(VI) on montmorillonite with different initial concentrations of U(VI), and the value of ΔG was smaller higher temperatures, indicating that the process of U(VI) adsorption on montmorillonite was spontaneous [39].

SEM–EDS analyses

There was no noticeable change on the surface of kaolinite after the adsorption of U(VI). The surface was enriched with a small amount of uranium with a relative content of about 1.77%, and the relative contents of O, Si, Al and other elements in the structure were slightly reduced after adsorption. It is inferred that adsorption of the U(VI) on kaolinite involve the base surface sites and side surface sites; the adsorption reaction with the base surface sites is an ion exchange process, and the adsorption reaction with the side surface sites is a surface complexation reaction [40].

The surface morphology of montmorillonite did not change significantly after the adsorption of U(VI), except that the overall profile of the montmorillonite was blurred after adsorption of U(VI), and a scan of the montmorillonite surface revealed that a large amount of uranium was gathered on the surface; the relative content was 3.67%. In contrast, the relative contents of Si, Al and the other elements had decreased after adsorption, and the adsorption of U(VI) on montmorillonite may also involve an ion exchange process.

FT-IR analyses

After adsorption of U(VI) by the kaolinite, the positions of the spectral peak in the low-frequency region (1300 cm^{-1}–400 cm^{-1}) changed. This region contains the characteristic Si–O stretching and bending vibrational bands of the clay minerals. The intensity of the spectral peak at 1036.01 cm^{-1} was enhanced. The peak at 1084.15 cm^{-1} was shifted to 1104.91 cm^{-1} for the inner Si–O bonding surface [41]. The stretching vibrations in this region indicated that the U(VI) ions underwent ion exchange or complexation reactions with the basal surface sites in the silica-oxygen skeleton of kaolinite, resulting in the adsorption of U(VI) ions.

The positions of the three absorption peaks located near 3683.02 cm^{-1}, 2920 cm^{-1} and 2853.84 cm^{-1} in the high frequency region did not change significantly after adsorption of the U(VI) by montmorillonite, and the water bending vibration at 3415.04 cm^{-1} was an overtone of the water molecule bending vibration at 1647.68 cm^{-1} in the middle frequency region [42]. The absorption band near 3415.04 cm^{-1} was shifted to 3499.09 cm^{-1}, the peak shape was narrowed and the intensity increased, indicating that the water molecules entered the interlayer domain of montmorillonite during the adsorption process and generated

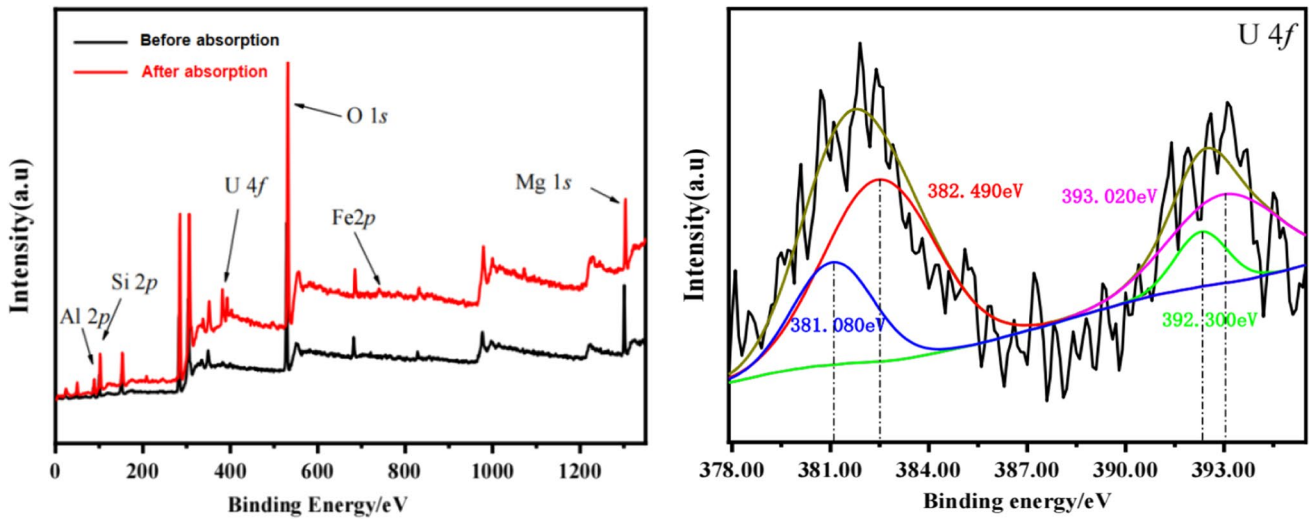

Fig. 16 XPS data for kaolinite after adsorption of U(VI). *Note* Background solution pH: 6.0 ± 0.1

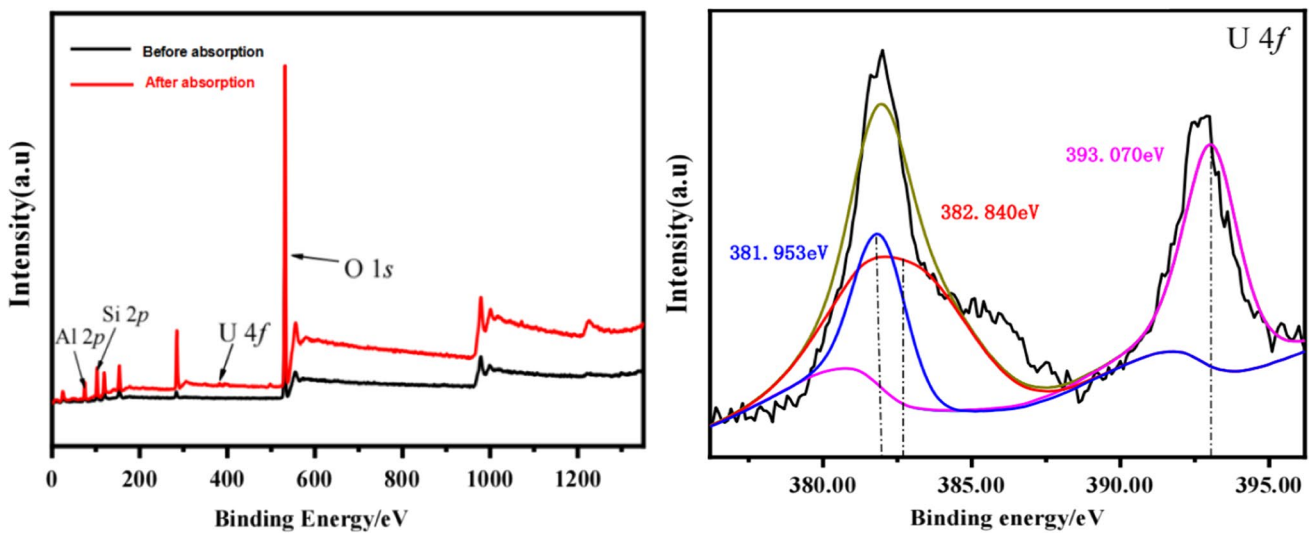

Fig. 17 XPS diagram for Montmorillonite after adsorption of U(VI). *Note* Background solution pH: 6.0 ± 0.1

strong water absorption peaks; the bending vibration of water molecules at 1647.68 cm^{-1} in the middle frequency region was shifted by 10 cm^{-1} and the intensity increased, further indicating that the water molecules entered the interlayer domain of montmorillonite. Additionally, the water molecule vibration near 3499.09 cm^{-1} was driven to increase. The water vibrational band near 3499.09 cm^{-1} was enhanced, and the faint spectral peak near 1375.59 cm^{-1} is an overtone of the water bending vibration at 1647.68 cm^{-1}; the Si–O stretching vibrational peaks at 1009.26 cm^{-1} ~ 1076.14 cm^{-1} for the silica-oxygen skeleton showed no noticeable changes. The Al–O and Si–O absorption peaks appeared near 626.97 cm^{-1} in the low-frequency region and corresponded to outer absorption peaks or bending vibrational peaks for Al–O–M and Si–O–M, suggesting that complexation reactions occurred during the adsorption of U(VI) on montmorillonite [43].

XPS analysis

Multiple U 4f peaks were observed in the binding energy range 375.00 eV–400.00 eV after U(VI) adsorption on kaolinite, indicating that the uranium was immobilized on kaolinite. The peaks at binding energies of 381.080 eV and

Table 1 Isothermal adsorption model fitting parameters for U(VI) adsorption by the clay minerals

Isothermal adsorption model	Fitting parameters	Clay minerals	
		Kaolinite	Montmorillonite
Langmuir model	R^2	0.99125	0.91321
	K_L	5.75E+04	9.29E+04
	Q_m	3.58E−05	6.57E−05
	RLmax	0.5665	0.4471
	RLmin	0.1228	0.0797
Freundlich model	K_F	1.37E−03	1.08E−02
	n	2.1790	1.92734
	R^2	0.96222	0.97184
Temkin model	K_T	5.03E+05	3.93E+05
	R^2	0.98349	0.86985
D-R model	Q_m	1.72E−04	6.34E−04
	E	1.26E+04	1.14E+04
	R^2	0.97465	0.96001

The significance of the italicized values in this Table 1 is crucial to the conclusion of the adsorption behavior after fitting the adsorption isotherms and kinetic models

Table 2 Kinetic model fitting parameters for U(VI) adsorption by the clay minerals

Kinetic model	Fitting parameters	Clay minerals	
		Kaolinite	Montmorillonite
Pseudo-first-order kinetic model	*qe*	2.18E−05	5.61E−05
	k1	7.26E−02	8.64E−01
	R^2	0.86585	0.99774
Pseudo-second-order kinetic model	*qe*	3.09E−05	5.73E−05
	K2	−13.6689	1.2575
	R^2	0.99977	0.99974
two-constant kinetic model	*k*	0.05415	0.2025
	R^2	0.7584	0.8469
Elovitch model	α	18.12	2.25E−4
	β	8.79E+05	1.13E+05
	R^2	0.78812	0.93436

The significance of the italicized values in this Table 2 is crucial to the conclusion of the adsorption behavior after fitting the adsorption isotherms and kinetic models

Table 3 Thermodynamic model fitting parameters for U(VI) adsorption by kaolinite

C_0 mol L^{-1}	ΔH J mol^{-1}	ΔS J mol^{-1} K^{-1}	ΔG/J mol^{-1}			R^2
			298.15 K	308.15 K	318.15 K	
1.26×10^{-5}	2.13E+04	74.26	−1.31E+03	−2.06E+03	−2.80E+03	0.9684
2.15×10^{-5}	1.79E+04	61.58	−5.03E+02	−1.12E+03	−1.73E+03	0.9748
3.00×10^{-5}	1.63E+04	54.66	−4.40E+01	−5.91E+02	−1.14E+03	0.9939
4.21×10^{-5}	1.31E+04	41.38	7.89E+02	3.76E+02	−3.82E+01	0.9644
6.35×10^{-5}	8.27E+03	23.31	1.31E+03	1.08E+03	8.49E+02	0.9596
8.22×10^{-5}	1.20E+04	33.13	2.09E+03	1.76E+03	1.43E+03	0.9999
1.27×10^{-4}	5.97E+03	10.45	2.86E+03	2.75E+03	2.65E+03	0.9889

392.300 eV were for U(IV) species. The peaks at binding energies of 382.490 eV and 393.020 eV were for U(VI) species of uranium [44], indicating some of the U(VI) was adsorbed as U(VI) on the kaolinite and some underwent reduction during the adsorption process to produce U(IV) on the kaolinite surface [45].

Table 4 Thermodynamic model fitting parameters for montmorillonite adsorption of U(VI)

C_0 mol L^{-1}	ΔH J mol^{-1}	ΔS J mol^{-1} K^{-1}	ΔG/J mol^{-1}			R^2
			298.15 K	308.15 K	318.15 K	
1.26×10^{-5}	1.16E+05	4.00E+02	−3.50E+03	−7.50E+03	−1.15E+04	0.9669
2.15×10^{-5}	7.71E+04	2.68E+02	−2.78E+03	−5.46E+03	−8.13E+03	0.9727
3.00×10^{-5}	6.61E+04	2.27E+02	−1.49E+03	−3.76E+03	−6.02E+03	0.9972
4.21×10^{-5}	4.22E+04	1.47E+02	−1.63E+03	−3.10E+03	−4.57E+03	0.9315
6.35×10^{-5}	4.31E+04	1.47E+02	−7.99E+02	−2.27E+03	−3.74E+03	0.9949
8.22×10^{-5}	2.25E+04	7.75E+01	−6.44E+02	−1.42E+03	−2.20E+03	0.9984
1.27×10^{-4}	9.73E+03	3.36E+01	−2.81E+02	−6.17E+02	−9.53E+02	0.8908

Montmorillonite contains Al, Si, O, Mg and other elements. Based on the XPS data, it was obvious that several U 4f peaks appeared in the binding energy range 375.00 eV–400.00 eV after the adsorption of U(VI) by montmorillonite, which indicated that the montmorillonite adsorbed U(VI). Fitting analyses of the curves revealed peaks for the U $4f_{7/3}$ state with binding energies of 381.953 eV and 382.840 eV and peaks for the U $4f_{5/3}$ state with binding energies of 393.070 eV, which corresponded to U(VI) species; this indicated that the U(VI) species adsorbed on montmorillonite had not undergone valence changes and were U(VI) complexes [46].

Conclusions

Many studies have shown that modified clay materials have good adsorption and removal efficiencies with various pollutants (Table 5). However, there are still gaps in the research on adsorption and removal of pollutants with natural clay minerals. In this study, the differences in the adsorption behaviors and adsorption mechanisms for natural montmorillonite and kaolinite with simulated uranium-contaminated groundwater were investigated to provide theoretical support for the feasibility of clay mineral remediation of groundwater pollutants in uranium mines.

The optimal pH ranges for U(VI) adsorption by montmorillonite and kaolinite were 4–7, 7–10, respectively. The adsorption U(VI) on montmorillonite was more efficient than that on kaolinite. The adsorption rates of the two minerals increased with increasing solid concentrations, and the amount of U(VI) adsorbed increased with higher initial concentrations and temperatures. In addition, the processes for adsorption of U(VI) on montmorillonite and kaolinite were controlled by chemical and physical effects. The spontaneous adsorption of U(VI) on the surface of montmorillonite was positively correlated with the temperature. The adsorption of low concentration U(VI) on kaolinite surface is a spontaneous reaction process, and the adsorption of high. The adsorption of dilute U(VI) on the kaolinite surface was a spontaneous process, and the adsorption of concentrated U(VI) on the kaolinite surface required heating.

The processes involved in adsorption of U(VI) on montmorillonite were mainly multilayer non-homogeneous adsorption or pore diffusion adsorption, and the adsorption of U(VI) on kaolinite occurred mainly via homogeneous monolayer adsorption. Both adsorption methods were ion exchange reactions. The SEM–EDS, FT-IR, and XPS results showed that the adsorption of U(VI) on montmorillonite and kaolinite occurred via ion-exchange reactions in the interlayer domain, base surface, and side surface, but also might have involved complexation reactions with active sites such as ≡SOH and $\equiv SO^-$ on the base surface or side surface; the adsorbed species were immobilized as $\equiv SOUO_2^{2+}$ or $\equiv SOUO_2OH$, etc. [51]. U(VI) did not undergo valence change during adsorption on montmorillonite, and during adsorption on kaolinite, U(VI) was reduced to U(IV). Overall, this study shows that there is a differential adsorption of U(VI) by natural montmorillonite and kaolinite for and

Table 5 Progress in the studies of U(VI) adsorption by clay minerals [47–50]

	Adsorbent material	Maximum saturated adsorption capacity	Maximum adsorption rate (%)
1	Montmorillonite	2.612 mg g^{-1}	85
2	Kaolinite-based composite	6.56×10^{-5} mol g^{-1}	70
3	Kaolinite titanium hydroxide composite	161.5 mg g^{-1}	16.5
4	Kaolinite and illite	–	96
This study	Montmorillonite and kaolinite	6.78×10^{-5} mol g^{-1}	78.68

that both have good potential as adsorbents for contaminated groundwater from uranium mines.

Acknowledgements The authors are extremely thankful to the anonymous reviewers that work in this paper.

Funding National Natural Science Foundation of China (No. 42272301). Open Fund Project of State Key Laboratory of Nuclear Resources and Environment, East China University of Technology (No.2020NRE18). Foundation for Educational Commission of Jiangxi Province of China (No. GJJ200720). Open Fund of National Defense Key Discipline Laboratory of Radioactive Geology and Exploration Technology (No. 2020RGET08).

Declarations

Conflict of interest The authors declare no conflicts of interest.

Ethical approval Not applicable.

Consent to participate Not applicable.

Consent for publication Not applicable.

References

1. Minas F, Chandravanshi BS, Leta S (2017) Chemical precipitation method for chromium removal and its recovery from tannery wastewater in Ethiopia. Chem Int 3(4):291–305
2. Kharecha PA, Hansen JE (2013) Prevented mortality and greenhouse gas emissions from historical and projected nuclear power. Environ Sci Technol 47:4889–4895
3. Xun Y, Xuegang L (2015) Radionuclides distribution, properties, and microbial diversity of soils in uranium mill tailings from southeastern China. J Environ Radioact 139:85–90
4. Sun Z, Chen D, Chen B, Kong L, Su M (2018) Enhanced uranium(VI) adsorption by chitosan 394 modified phosphate rock. Colloid Surf A 547:141–147
5. Chen S, Wei X, Liu J, Sun Z, Chen G, Yang M, Liu Y, Wang D, Ma C, Kong D (2022) Weak acid leaching of uranium ore from a high carbonate uranium deposit. J Radioanal Nucl Chem Int J Deal Asp Appl Nucl Chem 6:331
6. Orozco I, Romero M, Lara R, Bazan V (2018) Precipitation of uranium from alkaline liqueurs. Matéria 23:3336
7. Rong L, Zeming S, Yun H, Kailiang Z, Lvhang Y (2019) Uranium sorption onto mullite: characteristics of isotherms, kinetics and thermodynamics. J Earth Syst Sci 128(7):176–179
8. Sar SK, Diwan V, Biswas S, Singh S, Sahu M, Jindal MK, Arora A (2018) Study of uranium level in groundwater of Balod district of Chhattisgarh state, India and assessment of health risk. Hum Ecol Risk Assess 24:691–698
9. Yang H, Luo X, Ding H, Zhang X (2018) Adsorption of U(VI) by elodea nuttallii: equilibrium, kinetic and mechanism analysis. J Radioanal Nucl Chem 319(4):227
10. Hamutoko JT, Mapani BS, Ellmies R, Bittner A, Kuells C (2014) A fngerprinting method for the identifcation of uranium sources in alluvial aquifers: an example from the Khan and Swakop Rivers, Namibia. Phys Chem Earth 72–75:34–42
11. Nada FT, Laith AN, Enas MY (2014) Uranium concentration and its associated health hazards in drinking water of Nineveh Province (Iraq). World Appl Sci J 31(11):1938–1944
12. Borch T, Roche N, Johnson TE (2012) Determination of contaminant levels and remediation efficacy in groundwater at a former in situ recovery uranium mine. J Environ Monit JEM 14(7):1814–1823
13. Obiri-Nyarko F, Grajales-Mesa SJ, Malina G (2014) An overview of permeable reactive barriers for in situ sustainable groundwater remediation. Chemosphere 111:243–259
14. LIZhang JY (2012) Remediation technology for the uranium contaminated environment: a review. Proc Environ Sci 13:1609–1615
15. MaZhang JY (2006) Simultaneous sorption of phosphate and phenanthrene to inorgano-organo-bentonite from water. J Hazard Mater 136(3):982–988
16. Ma L (2014) Als-pill ared montmorillonite modifed by cationic and zwitterionic surfactants: a comparative study. Appl Clay Sci 101:327–334
17. Diwan V, Sar SK, Biswas S, Lalwani R (2020) Adsorptive extraction of uranium(VI) from aqueous phase by dolomite. Groundw Sustain Dev 11:100424
18. Kornilovych B, Kovalchuk L, Tobilko V, Ubaldini S (2020) Uranium removal from groundwater and waste water using clay-supported nanoscale zero-valent iron. Metals 10:111–116
19. Xiong H, JieminZhang T, WenzhongHuang C, YulingHu B (2021) Unexpected ultrafast elimination of uranium and europium from aqueous solutions with magnetic bio-$CaCO_3$. J Mol Liquids 322(1):114986
20. Khan S, Anjum R, Bilal M (2021) Revealing chemical speciation behaviors in aqueous solutions for U(VI) and europium (III) adsorption on zeolite. Environ Technol Innov 22:101503
21. Gladysz-Plaska A (2019) Adsorption properties of sepiolite in relation to Uranium and Lanthanide lons. Imerals 5:20–31
22. Bergaya F, Lagaly G (2006) Chapter 1 general introduction: clays, clay minerals, and clay science. Dev Clay 1(05):1–18
23. Zhu R, Chen Q, Zhou Q, Xi Y, Zhu J, He H (2016) Adsorbents based on montmorillonite for contaminant removal from water: a review. Appl Clay Sci 123:239–258
24. Kralik M (2014) Adsorption, chemisorption, and catalysis. Chemicke Zvesti 68(12):1625–1638
25. Zhang N, Lin LS, Gang DC (2008) Adsorptive selenite removal from water using iron-coated GAC adsorbents. Water Res 42:3809–3816
26. Liu B, Sun H, Peng T, Duan T (2019) Transport and transformation of uranium and heavy metals from uranium tailings under simulated rain at different pH. Environ Chem Lett 18:10
27. Wang X (2016) Study on the adsorption behavior of Th(IV) and U(VI) on two different illites[D]. Lanzhou University
28. Grim RE (1953) Clay mineralogy. McGraw-Hill, New York
29. Majd MM, Kordzadeh-Kermani V, Ghalandari V, Askari A, Sillanp M (2022) Adsorption isotherm models: a comprehensive and systematic review (20102020). Sci Total Environ 812:151334–152338
30. Kapnisti M, Noli F, Misaelides P, Vourlias G, Karfaridis D, Hatzidimitriou A (2018) Enhanced sorption capacities for lead and uranium using titanium phosphates; sorption, kinetics, equilibrium studies and mechanism implication. Chem Eng J 342:184–195
31. Yang C, Zhong Y, Li L, Ren X, Sun Y, Niu D, Liu Y, Yin M, Zhang D (2018) Lead and uranium sorption characteristics on hydrothermal synthesized delta manganese dioxide. J Radioanal Nucl Chem Int J Deal Aspect Appl Nucl Chem 317(3):1399–1408
32. Wang J, Guo X (2020) Adsorption kinetic models: physical meanings, applications, and solving methods. J Hazard Mater 15(390):122156
33. Noreen S, Kausar A, Zaman Q, Bhatti H, Nawaz I (2016) Efficient remediation of zr(IV) using citrus peel waste biomass: kinetic, equilibrium and thermodynamic studies. Ecol Eng J Ecotechnol 95:216–228

34. Ali SI, Lalji SM, Awan Z, Hashmi S, Khan G, Asad M (2022) Comprehensive performance analysis of kinetic models used to estimate asphaltene adsorption kinetics on nanoparticles. Chem Papers 77:1–15
35. Lebedeva OV, Sipkina EI et al (2016) Adsorption of Platinum(IV) by a composite based on silicon dioxide and copolymer of 4-Vinylpyridine and 2-Hydroxyethylmethacrylate. Protect Metals Phys Chem Surf 53(2017):80–84
36. Cheira MF, Mira HI, Sakr AK, Mohamed SA (2019) Adsorption of U(VI)from acid solution on a low-cost sorbent: equilibrium, kinetic, and thermodynamic assessments. Nucl Technol Engl 30(10):18
37. Meng F, Yuan G, Larson SL, Ballard JH, Han FX (2019) Kinetics and thermodynamics of uranium (VI) adsorption onto humic acid derived from leonardite. Int J Environ Res Public Health 16(9):1552
38. Tseng KNT, Kampf JW, Szymczak NK (2015) On the mechanism of n,n,n-amide ruthenium(II) hydride mediated acceptorless alcohol dehydrogenation: inner-sphere β-h elimination vs. outer-sphere bifunctional metal-ligand cooperativity. Acs Catal, 150810145618005
39. Gado MA, Atia BM, Hagag MS (2020) Kinetics and thermodynamics of uranium adsorption using impregnated magnetic graphene oxide. Iran J Chem Chem Eng Int Engl Edn 39:225
40. Elhefnawy OA, Elabd AA (2017) Optimization of uranyl ions removal from aqueous solution by natural and modified kaolinites. Radiochim Acta 105:609
41. Li JH, Liu WG, Zhang ZM, Li HN, Jiang QF, Wang YC, Tang RJ, Xu B, Guo RH, Su XB, Hua R (2022) Adsorption of uranium on amino functionalized acrylonitrile anion exchange resin. J Radioanal Nucl Chem 331(12):5771–5779
42. Peng TQ, Wang YF, Xu YF, Liu ZC (2023) Synthesis, characterization and uranium (VI) adsorption mechanism of novel adsorption material poly(tetraethylenepentamine-trimesoyl chloride). J Radioanal Nucl Chem 332(2):409–422
43. Vahur S et al (2021) Quantitative mineralogical analysis of clay-containing materials using atr-ft-ir spectroscopy with pls method. Anal Bioanal Chem 26:6535
44. Zhu M, Liu L, Feng J, Dong H, Zhang C, Ma F, Wang Q (2021) Efficient uranium adsorption by amidoximized porous polyacrylonitrile with hierarchical pore structure prepared by freeze-extraction. J Mol Liquids 328:115304
45. Jing C, Li Q, Tang Z, Xu J, Li Y (2019) Removal of soluble uranium by Illite supported nanoscale zero-valent iron: electron transfer processes and incorporation mechanisms. J Radioanal Nucl Chem 323:2016
46. Peng TQ, Wang YF, Xu YF, Liu ZC (2023) Synthesis, characterization and uranium (VI) adsorption mechanism of novel adsorption material poly(tetraethylenepentamine-trimesoyl chloride). J Radioanal Nucl Chem 332:1–14
47. Zhou W, Wang J, He J, Yang X, Liu C (2019) Adsorption of U(VI) on montmorillonite in the presence of ethylenediaminetetraacetic acid. Colloids Surf A 583:123929
48. Senol ZM, Keskin ZS, Ozer A, Simsek S (2022) Application of kaolinite-based composite as an adsorbent for removal of uranyl ions from aqueous solution: kinetics and equilibrium study. J Radioanal Nucl Chem Int J Deal All Aspect Appl Nucl Chem 1:331
49. Hagag MS, Esmaeel SMA, Salem F, Ali AH, Zaki SA (2022) Thermal activation of kaolinite titanium hydroxide composite for uranium adsorption from aqueous solutions. Int J Environ Sci Technol 3:1–12
50. Geng R, Yuan L, Shi L, Qiang S, Li Y, Liang J, Li P, Zheng G, Fan Q (2022) New insights into the sorption of U(VI) on kaolinite and illite in the presence of aspergillus niger. Chemosphere 288:132497
51. Wu J, Zheng Z, Zhu K, Xiang C, Wang J, Liu J (2022) Adsorption performance and mechanism of g-c3n4/uio-66 composite for u(vi) from aqueous solution. J Radioanal Nucl Chem 331(1):469–481

Publisher's Note Springer Nature remains neutral with regard to jurisdictional claims in published maps and institutional affiliations.

Springer Nature or its licensor (e.g. a society or other partner) holds exclusive rights to this article under a publishing agreement with the author(s) or other rightsholder(s); author self-archiving of the accepted manuscript version of this article is solely governed by the terms of such publishing agreement and applicable law.